

Hierarchical Planning for Long-Horizon Manipulation with Geometric and Symbolic Scene Graphs

Yifeng Zhu^{1,2}, Jonathan Tremblay¹, Stan Birchfield¹, Yuke Zhu^{1,2}

Abstract—We present a visually grounded hierarchical planning algorithm for long-horizon manipulation tasks. Our algorithm offers a joint framework of neuro-symbolic task planning and low-level motion generation conditioned on the specified goal. At the core of our approach is a two-level scene graph representation, namely *geometric scene graph* and *symbolic scene graph*. This hierarchical representation serves as a structured, object-centric abstraction of manipulation scenes. Our model uses graph neural networks to process these scene graphs for predicting high-level task plans and low-level motions. We demonstrate that our method scales to long-horizon tasks and generalizes well to novel task goals. We validate our method in a kitchen storage task in both physical simulation and the real world. Our experiments show that our method achieved over 70% success rate and nearly 90% of subgoal completion rate on the real robot while being four orders of magnitude faster in computation time compared to standard search-based task-and-motion planner. Additional material at <https://zhuyifengzhu.github.io/projects/hierarchical-scene-graph>

I. INTRODUCTION

Long-term robot autonomy in everyday environments demands a robot to make autonomous decisions over prolonged time periods. It is typically cast as a sequential decision making problem where a robot searches for feasible *plans* as sequences of actions in a finite horizon. In robot manipulation, a fundamental challenge stems from the high-dimensional search space of continuous robot actions, exacerbated by the combinatorial growth of planning complexity with respect to the task length.

A common approach to tackling long-horizon tasks is task-and-motion planning (TAMP) that factorizes the planning process into discrete symbolic reasoning and continuous motion generation [5, 16, 23, 30, 31]. However, several challenges present in classical TAMP methods, hindering their practical applicability in real-world domains: 1) these methods rely on manually specified symbolic rules, namely planning domains; 2) they typically abstract away raw perception with known physical states; 3) searching with discrete symbols and continuous motions remains prohibitively expensive in complex domains.

Over the past few years, a rising number of data-driven methods have been developed for robotic planning. Most notably, deep learning techniques have demonstrated their effectiveness in end-to-end learning of sensor-space models [9, 26] or latent-space models [8, 11, 36] for planning and control. These methods excel at integrating raw sensory input and generating reactive behaviors, but fall short of the

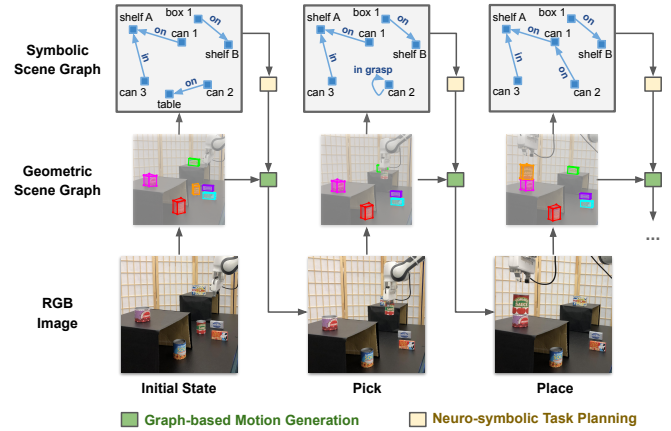


Fig. 1: We introduce a hierarchical planning model for vision-based long-horizon manipulation. We represent a manipulation scene with object-centric scene graphs at both geometric and symbolic levels, which can be used for neuro-symbolic task planning and graph-based motion generation respectively.

generalization capabilities for long-horizon tasks in comparison to TAMP algorithms. This dichotomy has ignited a series of work on integrating learning into the TAMP paradigm to speed up the search of feasible plans [3, 17, 35] or to directly predict the plan feasibility from an initial image [6]. However, these models still rely on strong domain knowledge and costly search procedures required by TAMP methods.

To tackle the challenges present in long-horizon planning problem, we introduce a visually grounded hierarchical planning algorithm for long-horizon manipulation tasks. Our algorithm operates directly on the visual observations and performs high-level task planning and low-level motion generation conditioned on a specification of the task goal. Through a novel combination of neural network-based learning and symbolic reasoning, our approach eliminates the need of predefined symbolic rules and complex motion planning procedures in TAMP. And by operating on our proposed graph-based representations, it attains a form of strong generalization to longer task instances which are difficult for end-to-end learning approaches.

At the heart of our approach is the structured object-centric representation of visual scenes. We propose to represent a manipulation scene as *scene graphs* [1, 28], a two-level abstraction shown in Figure 1. The low level is a *geometric scene graph* depicting the 6-DoF poses of the entities in the environment and their relative spatial relations. The high level is a *symbolic scene graph* that describes the abstract semantic relations among the entities and the robot. We obtain the two-level object-centric scene graphs of real-world

¹NVIDIA, ²The University of Texas at Austin.

household objects with the state-of-the-art 6D pose estimation models from RGB cameras [33] and symbol mapping. This hierarchical scene graph representation operates along with our hierarchical planning algorithm.

At each step in a manipulation process, current symbolic scene graph is used for a neuro-symbolic regression planner to determine the next immediate subgoal from the final goal specification. The regression approach frees us from massive time of searching while not requiring predefined symbolic rules as in TAMP. Then the subgoal is used for grounding with geometric scene graphs, opening the door for predicting parameterized motion parameters to reach the subgoal directly on this grounded geometric scene graph using graph-based motion generation. To enable neuro-symbolic task planning and graph-based motion generation, we integrate recent advances in learning-based neuro-symbolic reasoning [4, 38] and object-centric dynamics model learning [18, 40]. Both the task planning and motion generation models are based off the Graph Neural Networks (GNNs) [13] which are deep learning modules for graph processing.

Summary of Contributions: 1) We introduce a visually-grounded hierarchical planning algorithm that scales to long-horizon tasks through the use of two-level scene graph representations; 2) We design graph-based learning models and training procedures that enable our models to generalize to novel tasks; and 3) We demonstrate the effectiveness of our approach in tabletop manipulation tasks in both a simulated environment and the real world.

II. RELATED WORK

Task and Motion Planning. Our approach to factorizing long-term manipulation planning into the task level and the motion level has a strong resemblance to task-and-motion planning (TAMP) methods [5, 16, 23, 30]. Classic TAMP approaches rely on predefined symbolic rules and known dynamic models. They perform discrete task plans with logic search and continuous motion plans through sampling-based techniques [10, 16] or trajectory optimization [23, 31, 32]. TAMP methods can generalize to arbitrary goals defined in a problem domain; however, it suffers from the combinatorial complexity of searching for valid plans. Learning techniques [3, 17, 35] have been increasingly employed into the TAMP framework to accelerate inference, replacing handcrafted search heuristics. They aim to guide the search procedure towards more promising task plans, reducing the number of motion planning problems required to be solved. Alternatively, recent work has explored learning techniques to evaluate the feasibility of plans from visual observations [6, 37]. Most relevant to us is Deep Visual Reasoning [6] which directly predicted task plans from initial scene images. However, it predicted the task plan solely based on the initial image, and relied on environment dynamics for costly trajectory optimization. In contrast, our model performs regression task planning and achieves high inference efficiency by predicting both the task plans and motion plans with GNN-based models.

Learning to Plan. This work is also closely related to recent

efforts on learning to plan with end-to-end deep learning [8, 9, 11, 12]. The core idea is to learn predictive models from data which can be used for model-based reinforcement learning or planning. The dynamic models can be learned in raw sensor space [9, 24, 26] or learned latent space [8, 11, 12]. A major advantage of these models is that they can integrate seamlessly with neural representations learned from real-world sensory data and requires less domain knowledge than TAMP algorithms. However, the ability of making accurate long-term predictions would require a strong generalization capability generally beyond generic neural network models. To mitigate this problem, hierarchical structures have been introduced to neural network methods [8, 22, 24, 25, 27]. Like ours, these methods decompose a plan into high-level subgoals and low-level motions. Harnessing the temporal abstraction, these methods have been able to make long-horizon predictions for multi-stage tasks and generalize well to tasks within the training distributions. However, the neural representations have suffered from their limited generalization power to out-of-distribution or longer tasks. Inspired by the TAMP structure, recent works have looked into neuro-symbolic models for robotic planning [14, 15, 38] that exploit the complementary strengths of neural representations and symbolic representations. Among these methods, Regression Planning Network (RPN) [38] extended the classical regression planning in symbolic space with deep networks, achieving strong zero-shot generalization to unseen tasks. However, RPN simplified perception as 2D object bounding boxes and abstracted away low-level motions. Our model adopts a similar regression planning technique on the task level, and moreover, directly interfaces with a low-level motion generation module through the hierarchical scene graph representations from real images.

Graph-based Scene Representations. A key factor determining the generalization capability of a planning model is the choice of state representations. Many works have demonstrated that factorized representations of objects and entities improve a model’s ability to reason about novel scene and new tasks [2, 7, 18, 21]. For robot manipulation, the entities and their relations in the environment supply essential information for planning a robot’s actions. This has motivated a variety of graph-based scene representations [1, 19, 28, 29, 39] developed in the robotics and computer vision community. These representations have been used in prior work of robotic manipulation for short-term skill learning [29, 40] or high-level task planning [38]. Instead, we integrate the scene graph representations at the two levels of abstraction to offer a coherent framework of task planning and motion generation. In a similar vein, different forms of hierarchical 3D scene graph representations [1, 28] have been developed in the 3D vision and SLAM communities. Our key novelty, in comparison, is to make use of our hierarchical representations for visual planning.

III. PROBLEM STATEMENT

Here we consider a vision-based goal-conditioned planning problem. Let \mathcal{O} be the space of raw visual observations,

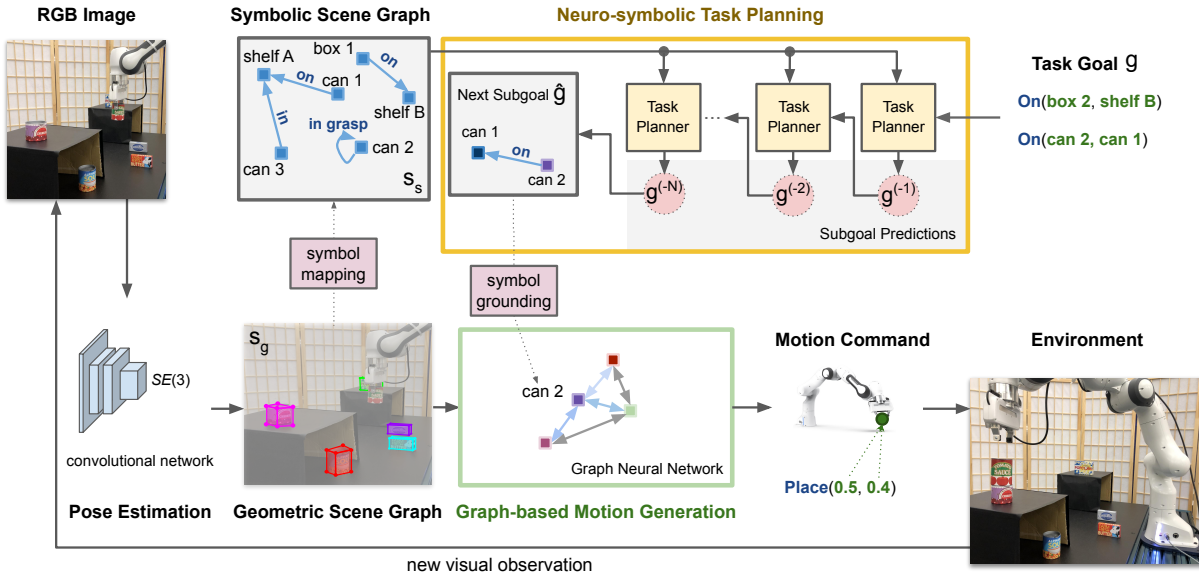


Fig. 2: An overview of our scene graph-based hierarchical planner. 1) Given an observation o of the environment, we use a CNN based pose estimator $f_p(o)$ to obtain poses of objects. 2) We construct the geometric scene graph s_g using output from pose estimation. We omit edge connections for the graph in figure. 3) A symbol mapping function f_m maps from s_g to s_s . 4) A symbolic goal is given to the task planner, and the task planner recursively predicts subgoals g^{-i} until the next immediate subgoal \hat{g} . 5) The geometric scene graph s_g is grounded with next immediate subgoal \hat{g} and motion generation model takes in the grounded graph and the next immediate subgoal to command low-level motor control for robot to execute a primitive such as pick, place, or push.

\mathcal{A} be the action space of robot motor control, and \mathcal{G} be the space of goal specifications, the goal of our algorithm is to find a policy $\pi : \mathcal{O} \times \mathcal{G} \mapsto \mathcal{A}$ to generate low-level motor action $a \in \mathcal{A}$ given the current observation $o \in \mathcal{O}$ and a goal $g \in \mathcal{G}$. In complex manipulation tasks, it takes a prolonged sequence of low-level actions to achieve a long-term goal, making the planning problem computationally prohibitive. To overcome this challenge, we factorize the problem into high-level task planning and low-level motion generation.

We design two-level scene graphs as the representation for our factorization of the problem (see Figure 2). On the low level, a *geometric scene graph* s_g , similar to kinematic graph [20], describes the Cartesian locations of objects. Each node defines the pose of an object in $SE(3)$, and each edge defines the relative spatial relations between two objects. A geometric scene graph s_g can be computed from a visual observation $o \in \mathcal{O}$ with a 6-DoF *pose estimation* model f_p where $s_g = f_p(o)$. On the high level, we use a vocabulary of semantic symbols to form an abstract description of a scene, allowing us to express both the current state and the goal specification with logical predicates. A *symbolic scene graph* s_s is thus a set of visually grounded predicates that characterizes the object states and the semantic relations between objects. Later we refer to nodes or objects interchangeably. Given a geometric scene graph, we can design a *symbol mapping* function f_m to compute its corresponding symbolic scene graph $s_s = f_m(s_g)$. Let \mathcal{Z} be the space of all possible sets of predicates. In this case, we have $s_s \in \mathcal{Z}$ and $\mathcal{G} \subset \mathcal{Z}$. Our hierarchical planning process is to learn a task planning model ϕ and a motion generation model ψ where

$$\phi : \mathcal{Z} \times \mathcal{G} \rightarrow \mathcal{G} \quad (1)$$

$$\psi : \mathcal{O} \times \mathcal{G} \rightarrow \mathcal{A}. \quad (2)$$

The task planning model ϕ takes a symbolic scene graph $s_s \in \mathcal{Z}$ and a task goal $g \in \mathcal{G}$ as input, and predicts the next subgoal $\hat{g} \in \mathcal{G}$, namely an immediate subgoal that can be achieved by a single motion primitive (see Section IV-A). Subgoals are the necessary intermediate states to be achieved before reaching the goal g . The motion generation model ψ computes s_g from $o \in \mathcal{O}$, processes s_g and \hat{g} with a *symbol grounding* function f_g , and generates a low-level action $a \in \mathcal{A}$ (see Section IV-B).

IV. METHOD

We provide an overview of our model in Figure 2. From the current RGB observation, our model constructs a hierarchical representation of the geometric scene graph and the symbolic scene graph. At the high level, it performs neuro-symbolic task planning and predicts the next symbolic subgoal conditioned on the current symbolic scene graph and the specified goal. At the low level, it performs forward motion generation by grounding the symbolic subgoal to the current geometric scene graph and predicting motion parameters. Once the next subgoal is achieved, it replans according to this procedure with the new observation. As both levels directly operate on structured scene graphs, it makes Graph Neural Networks (GNNs) [13] a natural choice for our model architecture. GNNs are a family of geometric deep learning models for graph processing with the relational inductive biases for stronger generalization. A GNN learns features for each graph node and for each graph edge with parameter-shared modules (neural networks) and uses a message passing mechanism to exchange information among nodes in the local neighborhood. This design enables the model to aggregate contextual information through the graph structure while generalizing to different graph topologies,

such as different number of objects in our scene graphs.

A. Task Planning

Our task planning model ϕ is built on top of Regression Planning Networks (RPN) [38], which performs neuro-symbolic regression (backward) planning in the symbolic space using deep networks. Given a specification of the final task goal g , we denote its previous subgoal $g^{(-1)}$, and similarly, $g^{(-i-1)}$ as the previous subgoal of a subgoal $g^{(-i)}$. The core idea of regression planning is to recursively predict $g^{(-1)}$, $g^{(-2)}$ from g and s_s , all the way till a predicted subgoal $g^{(-N)}$ is *reachable*, that is, this subgoal can be achieved from the current state with a single motion primitive (see Section IV-B). We refer to this next immediate subgoal as \hat{g} . This approach for task planning has two major benefits: 1) Regression planning searches in a backward fashion, significantly reducing the search space compared to forward search. 2) The model can be trained on demonstrations of shorter tasks without predefined symbolic rules while generalizing to longer unseen tasks.

The task planning model ϕ has three key components: preimage network f_{preimage} , subgoal serialization, and reachability network f_{reach} . f_{preimage} takes a goal g or a subgoal $g^{(-i)}$ as inputs, and predicts all possible previous subgoals. This is achieved by predicting every edge relation in symbolic scene graph that needs to be satisfied preceding current subgoal in query, forming a preimage symbolic scene graph. f_{preimage} is a GNN model which uses a message passing mechanism to predict relations between every pair of nodes in the preimage graph. The subgoal serialization function then takes in all possible subgoals from the preimage graph, and selects one subgoal for subsequent reachability check. In contrast to RPN which uses a dependency network for selection, we uniformly sample a next subgoal among all possible next subgoals from as we find this effective.

After a possible subgoal is selected, f_{reach} checks if this subgoal is reachable from the current state with a single motion primitive. Specifically, we check if every target semantic relation of objects in the subgoal can be achieved or not. f_{reach} is also a GNN model, which predicts a binary label of whether the target semantic relation can be achieved. If the next subgoal is reachable, a motion primitive is selected based on the next subgoal. Otherwise, the whole process is repeated again, using $g^{(-i)}$ as inputs to f_{preimage} until finding a reachable immediate subgoal $\hat{g} = g^{(-N)}$.

B. Motion Generation

Our motion generation model ψ operates on the graph representations, including the immediate subgoal \hat{g} and the current geometric scene graph s_g , to compute a low-level motor command a to execute. We use a set of parametrized motion primitives π_θ to represent low-level motions (see details in Section V). The action space \mathcal{A} thus contains the continuous values θ that parametrize the motion primitives.

Our model first selects a motion primitive type based on the next symbolic subgoal \hat{g} . It can be done by a simple and effective heuristic that we adopt in this work. We then

ground \hat{g} to the geometric scene graph s_g by computing new, object-centric attributes for each node relative to the object or target region in \hat{g} . This results in a grounded geometric scene graph \hat{s}_g , where the node attributes that are specific for the next subgoal. \hat{s}_g captures contextual information of other objects, which is important for the motion primitive to avoid collisions and determines the execution trajectories given the constraints imposed by the environment. We encode these constraints of the environment using a GNN model on \hat{s}_g .

The input to our motion generation model is comprised of the grounded geometric scene graph \hat{s}_g and the next immediate subgoal \hat{g} . It outputs parameters θ for the selected motion primitive. To predict θ conditioned on \hat{s}_g and \hat{g} , we first compute embedding vectors for \hat{s}_g using a GNN and \hat{g} using a fully-connected layer network separately, and then concatenate two embedding vectors and pass into a multilayer perceptron (MLP) to predict θ . Node attributes are specific to task design and motion primitive types. For different motion primitives, we design different object-centric node attributes in \hat{s}_g .

C. Scene Graph Generation

Our scene graphs contain both predefined environment fixtures, such as table and shelves, and small dynamic objects, such as cans and boxes, that can be manipulated by the robot. The poses of the dynamic objects are computed through a 6-DoF pose estimator. The pose estimator is a convolutional neural network, which takes an RGB image as input and predicts the $SE(3)$ pose of an object. We thus construct a geometric scene graph s_g by estimating the poses of individual objects, where each node represents an object and its node attributes represent the object's 6-DoF pose and its object type. Geometric scene graph is a fully connected graph where all nodes are connected to each other so that message passing in GNN can be done across all nodes, fully encoding constraints in the environment.

Once we have the geometric scene graph s_g , the symbol mapping function f_m generates symbolic predicates for edges in s_g and ignores geometric information in every node, forming the corresponding symbolic scene graph s_s . This symbol mapping also adds information of environment fixtures and robot's state into s_s for generating semantic relations. We leverage the robot's state such as whether an object is being held by the robot, in the symbolic scene graph to compute these robot-related predicates. In practice, f_m can be either manually defined or learned [15]. For our manipulation domains, we manually define the function for simplicity. In the resultant graph, each node describes the object type and each edge describes the symbolic relations. As semantic relations are usually asymmetric, we use directed edges to represent symbolic relation between object nodes and subject nodes. To represent unary predicates, we add self edges to the nodes. We provide details about the logical predicates used in our tasks in Section V-A.

D. Model Training

We train our task planning module using a set of short task demonstrations. For simplicity, we use an algorithmic plan-

ner to automate the process of generating demonstrations. Once collecting trajectories of demonstrations, we generate symbolic scene graphs of each state, obtaining the state transitions in symbolic space. For training f_{preimage} , we use pairs of subsequent symbolic scene graphs from demonstration sequences. As we have mentioned in f_{preimage} design, it predicts the preimage graph of a subgoal. Therefore during training, we directly provide previous symbolic scene graph as supervision for training. For training f_{reach} , we use pairs of subsequent symbolic scene graphs as well, but as we only have positive examples from demonstration, we augment the data by altering predicates of edges in the next symbolic graphs, and use them as negative examples. Our label for reachability training is binary for each edge, predicting if a symbolic relation between two nodes or the unary predicate of a node is reachable or not from the current symbolic state.

To train our motion generation model ψ to predict parameters θ for motion primitives π_θ , we follow the self-supervised training procedure similar to CAVIN [8], learning from task-agnostic interactions. We procedurally generate random configurations of the environments in physical simulation, namely placements of objects, and collect training samples by sampling parameters of motion primitives and executing the sampled actions in simulation. The actions in successful execution are taken as training samples.

The pose estimator used in this work is DOPE [33], which is trained on a synthetic dataset of photo-realistic images, and each model predicts the $SE(3)$ pose of a known object from a single RGB image. Due to the massive domain randomization employed during training, it can give reliable pose estimations on real-world images.

V. EXPERIMENTS

A. Environment

We design a kitchen storage environment for experimental validation. It has two fixtures: shelf A on the left and shelf B on the right (see Figure 2). In our tasks, the robot manipulates one or several objects based on the goal specification, where the objects are specified to be inside the shelf, on the shelf, or on top of another object. We consider three types of motion primitives: `pick`, `place`, and `push`, execution of which are shown in Fig 3. We also define two regions on the table: open space in the middle and `prepush` regions in front of the shelves for objects to be pushed into a shelf. We use a selection of household objects from HOPE dataset [34], including three cans and three boxes, namely Cherries, AlphabetSoup, TomatoSoup and Popcorn, CreamCheese, Butter. We use DOPE [33] to estimate the poses of these objects for our real-world experiments. We build up our simulated environments based on robocat [8], a PyBullet-based simulation framework for robot manipulation. The experiments are conducted with a 7-DoF Franka Emika Panda robot arm.

a) Logical Predicates: In our tasks, we have four logical predicates for describing the symbolic states of objects: `InGrasp` describes the state when the object is in the robot’s gripper. `Clear` describes the state when the object is clear

to be grasped, or clear to be stacked on. `In` for objects inside the shelf, and `On` for objects on a region, a shelf or another object. With predicates defined, we can directly provide goals in symbolic forms like `On(Can, shelf A)`.

b) Motion Primitive Parametrization: In our task, we parameterize `place` with x, y locations in the environment, and discretize each dimension into 10 discrete bins. We parameterize `push` with θ for the angle to push and d for the distance to travel along the pushing angle. We also discretize each dimension, and we have 21 discrete bins for each. For simplicity, we do not predict the orientation for picking an object with `pick` or the position for stacking an object with `place`, but rather rely on the information from the geometric scene graph to determine the parameters.

c) Attributes for Grounded Scene Graphs: For `place`, grounding f_g assigns node features with its object type, object’s current region, and its pose relative to target region from \hat{g} . For `push`, grounded attributes for each node include its object type, its region, its pose relative to the object in \hat{g} , and its pose relative to shelf A.

B. Data Collection and Training Details

As we have mentioned, we train our task planning modules using a set of short demonstrations in our storage tasks. We only provide simple demonstrations of placing one object on a shelf, stacking two objects on a shelf, or pushing one object (can) into shelf A. We collect 18 trajectories of demonstration in total. For training our motion generation model, we collect all positive samples (successful execution) from sampled actions and create a dataset of 14,573 samples for `place` and 8,000 samples for `push` in simulation.

We train both task planning and motion generation models with cross entropy loss. For all shared modules in f_{preimage} and f_{reach} , we use a fully connected layer of 256 hidden units with LeakyReLU activations. For our motion generation model, we have two-round message passing in GNN to obtain the embedding from grounded scene graph \hat{s}_g and a fully-connected network to obtain embedding from subgoal \hat{g} . We use two-layer network for shared modules in the GNN model, with 256 hidden units for each layer. Both geometric embedding and symbolic embedding are 32-dimensional vectors. After concatenating two embeddings, we have another two-layer network with 256 hidden units for each layer to predict parameters of motion primitives.

C. Evaluation Setup

We evaluate our model on tasks with problem sizes ranging from two to six objects. In a task with n -object problem size, we have a goal specifying symbolic states of n objects. We exclude stacking objects cases for two-object problem size as they are provided in the demonstration.

We have two major evaluation metrics: success rate and subgoal completion rate. Success rate is the percentage of successful completion of the whole task out of all trials. Subgoal completion rate is the number of subgoals completed over the number of total subgoals in goal g to complete. Success rate tells us the overall performance of the model,

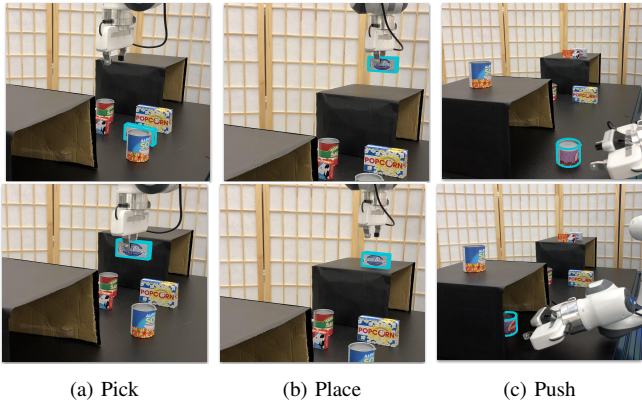


Fig. 3: Examples of the motion primitives used in our storage tasks.

while subgoal completion rate shows to what extent a task is completed even if it fails in the middle. We demonstrate the performance of our hierarchical planning framework by thorough evaluation with ground-truth poses in simulation, and validate its applicability in the real world by evaluating on the real robot with visual observation included.

D. Simulation Experiments with Ground-Truth Poses

We randomly generate 100 symbolic goal specifications (or fewer if all combinations are fewer) for each problem size, and for each goal specification, we evaluate five time repeatedly. To examine the strengths of our regression planning as opposed to direct forward prediction, we compare with a baseline method which directly predicts next subgoal conditioned on g and s_g using GNN models. Our results indicate that this direct subgoal prediction baseline has **zero** success rate for all problem sizes (thus not presented in the table), due to its inability of generalization to tasks longer than the training demonstrations. The performance of our approach is reported in Table I, along with two motion generation baselines: single-shot random sampling approach (Random), which uniformly samples a parameter from the parameter space, and a multi-layer perceptron approach (MLP), where we flatten all node attributes and edge attributes into a single vector, and use a fully-connected network of the same capacity as the GNN. We omit the standard deviations as all the standard deviation values are below 0.04. As the result suggests, our graph-based motion generation model is effective for single-shot prediction of θ compared to the random sampling baseline, and the relational inductive biases in GNNs boost performance as compared to the MLP baseline. Failure modes in our approach are primarily due to execution failure, and the rest are overstep failure. Execution failure refers to failure due to motion execution, and overstep failure is failure because of executing same motion primitives in infinity loop or never predicting a reachable subgoal within maximal steps of 50. We have 7.3% execution failure for problems of 2 objects, and all the way to 32.5% for problems of 6 objects.

A major advantage of our approach over classical TAMP method is its efficient inference for long-horizon tasks. The use of learning models substantially reduces the amount of

TABLE I: Success rate / subgoal completion rate in simulated environments with ground-truth poses: random sampling (Random), fully-connected network (MLP), and our method (Ours).

Problem Size	Random	MLP	Ours (GNNs)
2 objects	0.71 / 0.84	0.85 / 0.91	0.92 / 0.95
3 objects	0.60 / 0.81	0.75 / 0.87	0.89 / 0.95
4 objects	0.50 / 0.78	0.69 / 0.84	0.84 / 0.92
5 objects	0.35 / 0.67	0.56 / 0.76	0.73 / 0.87
6 objects	0.18 / 0.56	0.44 / 0.67	0.67 / 0.84

TABLE II: Computation time (in seconds) of the PDDLStream solver versus Ours (including RRT motion planning)

Problem Size	PDDLStream [10]		Ours	
	Task	Motion	Task	Motion
2 objects	127.9	23.5	0.15	18.1
3 objects	251.7	35.7	0.13	27.2
4 objects	251.2	62.9	0.22	36.5
5 objects	322.2	107.0	0.29	42.9
6 objects	424.2	276.9	0.32	49.4

search problems it has to solve. Table II shows a comparison of computation time against the state-of-the-art TAMP solver PDDLStream [10]. We found that our method significantly accelerates the inference procedure on both task and motion levels, especially for task planning, where the neuro-symbolic planner is four orders of magnitude faster than the search-based logic solver with PDDL.

E. Real Robot Experiments with Visual Observations

We evaluate our approach on the real robot with raw visual input. To achieve robust pose estimation results for computing the geometric scene scene, we take four images from different viewpoints around each region and each shelf respectively. Due to computation constraints, we evaluate 34 trials in total, including 10 trials for tasks consisting of 2 objects and 3 objects, 8 trials for 4 objects, 3 trials both for 5 objects and 6 objects. The overall success rate is **70.6%** and the subgoal completion rate is **89.6%**. The gap between the success rate and subgoal completion rate is due to execution failure of the motion primitives for the last few subgoals in large problem sizes. We show qualitative examples of our real-world experiments in the supplementary video.

VI. CONCLUSIONS

In this paper we present a visual hierarchical planning algorithm for long-horizon manipulation tasks. Our framework integrates neuro-symbolic task planning and graph-based motion generation on graph-based scene representations. The essence of our method lies in the two-level abstractions of a manipulation scene with *geometric scene graphs* and *symbolic scene graphs*. We show the good generalization ability to longer and novel tasks with models trained on a set of short demonstration. We quantitatively evaluate our approach in simulation and real-world experiments. Two promising directions are left for future work. One is how to learn the symbol mapping function in a self-supervised way from demonstration, which can further automate the framework and learning process. The other direction is to

develop a more flexible form of scene graph representations that can represent articulated and deformable objects.

ACKNOWLEDGEMENT

We would like to thank Guanya Shi for providing an improved version of DOPE. We also would like to thank Nvidia AI-Algorithm team for providing valuable internal feedback to the paper.

REFERENCES

- [1] I. Armeni, Z.-Y. He, J. Gwak, A. R. Zamir, M. Fischer, J. Malik, and S. Savarese, “3d scene graph: A structure for unified semantics, 3d space, and camera,” in *IEEE International Conference on Computer Vision*, 2019, pp. 5664–5673.
- [2] C. P. Burgess, L. Matthey, N. Watters, R. Kabra, I. Higgins, M. Botvinick, and A. Lerchner, “Monet: Unsupervised scene decomposition and representation,” *arXiv preprint arXiv:1901.11390*, 2019.
- [3] R. Chitnis, D. Hadfield-Menell, A. Gupta, S. Srivastava, E. Groshev, C. Lin, and P. Abbeel, “Guided search for task and motion plans using learned heuristics,” in *IEEE International Conference on Robotics and Automation (ICRA)*, 2016.
- [4] M. Cranmer, A. Sanchez-Gonzalez, P. Battaglia, R. Xu, K. Cranmer, D. Spergel, and S. Ho, “Discovering symbolic models from deep learning with inductive biases,” *arXiv preprint arXiv:2006.11287*, 2020.
- [5] N. T. Dantam, Z. K. Kingston, S. Chaudhuri, and L. E. Kavraki, “Incremental task and motion planning: A constraint-based approach,” in *Robotics: Science and systems*, Ann Arbor, MI, USA, vol. 12, 2016, p. 00052.
- [6] D. Driess, J.-S. Ha, and M. Toussaint, “Deep visual reasoning: Learning to predict action sequences for task and motion planning from an initial scene image,” *arXiv preprint arXiv:2006.05398*, 2020.
- [7] M. Engelcke, A. R. Kosiorek, O. P. Jones, and I. Posner, “Genesis: Generative scene inference and sampling with object-centric latent representations,” *arXiv preprint arXiv:1907.13052*, 2019.
- [8] K. Fang, Y. Zhu, A. Garg, S. Savarese, and L. Fei-Fei, “Dynamics learning with cascaded variational inference for multi-step manipulation,” *Conference on Robot Learning (CoRL)*, 2019.
- [9] C. Finn and S. Levine, “Deep visual foresight for planning robot motion,” *IEEE International Conference on Robotics and Automation (ICRA)*, pp. 2786–2793, 2017.
- [10] C. R. Garrett, T. Lozano-Pérez, and L. P. Kaelbling, “Pddl-stream: Integrating symbolic planners and blackbox samplers via optimistic adaptive planning,” in *Proceedings of the International Conference on Automated Planning and Scheduling*, vol. 30, 2020, pp. 440–448.
- [11] D. Hafner, T. Lillicrap, J. Ba, and M. Norouzi, “Dream to control: Learning behaviors by latent imagination,” in *International Conference on Learning Representations*, 2019.
- [12] D. Hafner, T. Lillicrap, I. Fischer, R. Villegas, D. Ha, H. Lee, and J. Davidson, “Learning latent dynamics for planning from pixels,” in *International Conference on Machine Learning*, 2019, pp. 2555–2565.
- [13] J. B. Hamrick, K. R. Allen, V. Bapst, T. Zhu, K. R. McKee, J. B. Tenenbaum, and P. W. Battaglia, “Relational inductive bias for physical construction in humans and machines,” *arXiv preprint arXiv:1806.01203*, 2018.
- [14] D.-A. Huang, Y.-W. Chao, C. Paxton, X. Deng, L. Fei-Fei, J. C. Niebles, A. Garg, and D. Fox, “Motion reasoning for goal-based imitation learning,” in *IEEE International Conference on Robotics and Automation (ICRA)*, 2020, pp. 4878–4884.
- [15] D.-A. Huang, D. Xu, Y. Zhu, A. Garg, S. Savarese, L. Fei-Fei, and J. C. Niebles, “Continuous relaxation of symbolic planner for one-shot imitation learning,” *arXiv preprint arXiv:1908.06769*, 2019.
- [16] L. P. Kaelbling and T. Lozano-Pérez, “Hierarchical task and motion planning in the now,” *IEEE International Conference on Robotics and Automation (ICRA)*, 2011.
- [17] B. Kim, Z. Wang, L. P. Kaelbling, and T. Lozano-Pérez, “Learning to guide task and motion planning using score-space representation,” *The International Journal of Robotics Research*, vol. 38, no. 7, pp. 793–812, 2019.
- [18] T. Kipf, E. van der Pol, and M. Welling, “Contrastive learning of structured world models,” in *International Conference on Learning Representations*, 2019.
- [19] R. Krishna, Y. Zhu, O. Groth, J. Johnson, K. Hata, J. Kravitz, S. Chen, Y. Kalantidis, L.-J. Li, D. A. Shamma, et al., “Visual genome: Connecting language and vision using crowdsourced dense image annotations,” *International journal of computer vision*, vol. 123, no. 1, pp. 32–73, 2017.
- [20] S. M. LaValle, *Planning algorithms*. Cambridge university press, 2006.
- [21] Z. Lin, Y.-F. Wu, S. V. Peri, W. Sun, G. Singh, F. Deng, J. Jiang, and S. Ahn, “Space: Unsupervised object-oriented scene representation via spatial attention and decomposition,” in *International Conference on Learning Representations*, 2020.
- [22] C. Lynch, M. Khansari, T. Xiao, V. Kumar, J. Tompson, S. Levine, and P. Sermanet, “Learning latent plans from play,” in *Conference on Robot Learning*, 2020.
- [23] T. Migimatsu and J. Bohg, “Object-centric task and motion planning in dynamic environments,” *IEEE Robotics and Automation Letters*, vol. 5, no. 2, pp. 844–851, 2020.
- [24] S. Nair and C. Finn, “Hierarchical foresight: Self-supervised learning of long-horizon tasks via visual subgoal generation,” in *International Conference on Learning Representations*, 2019.
- [25] S. Nasiriany, V. Pong, S. Lin, and S. Levine, “Planning with goal-conditioned policies,” in *Advances in Neural Information Processing Systems*, 2019, pp. 14 843–14 854.
- [26] J. Oh, X. Guo, H. Lee, R. L. Lewis, and S. Singh, “Action-conditional video prediction using deep networks in atari games,” in *Advances in neural information processing systems*, 2015, pp. 2863–2871.
- [27] K. Pertsch, O. Rybkin, F. Ebert, C. Finn, D. Jayaraman, and S. Levine, “Long-horizon visual planning with goal-conditioned hierarchical predictors,” *arXiv preprint arXiv:2006.13205*, 2020.
- [28] A. Rosinol, A. Gupta, M. Abate, J. Shi, and L. Carlone, “3d dynamic scene graphs: Actionable spatial perception with places, objects, and humans,” *arXiv preprint arXiv:2002.06289*, 2020.
- [29] M. Sieb, Z. Xian, A. Huang, O. Kroemer, and K. Fragkiadaki, “Graph-structured visual imitation,” in *Conference on Robot Learning*, 2020, pp. 979–989.
- [30] S. Srivastava, E. Fang, L. Riano, R. Chitnis, S. J. Russell, and P. Abbeel, “Combined task and motion planning through an extensible planner-independent interface layer,” *2014 IEEE International Conference on Robotics and Automation (ICRA)*, pp. 639–646, 2014.
- [31] M. Toussaint, “Logic-geometric programming: An optimization-based approach to combined task and motion planning,” in *IJCAI*, 2015, pp. 1930–1936.
- [32] M. A. Toussaint, K. R. Allen, K. A. Smith, and J. B. Tenenbaum, “Differentiable physics and stable modes for tool-use and manipulation planning,” 2018.
- [33] J. Tremblay, T. To, B. Sundaralingam, Y. Xiang, D. Fox, and S. Birchfield, “Deep object pose estimation for semantic

- robotic grasping of household objects,” in *Conference on Robot Learning*, 2018.
- [34] S. Tyree, J. Tremblay, T. To, J. Cheng, T. Mossier, and S. Birchfield, “6-DoF pose estimation of household objects for robotic manipulation: An accessible dataset and benchmark,” in *ICCV Workshop on Recovering 6D Object Pose*, 2019.
 - [35] Z. Wang, C. R. Garrett, L. P. Kaelbling, and T. Lozano-Pérez, “Active model learning and diverse action sampling for task and motion planning,” in *IEEE/RSJ International Conference on Intelligent Robots and Systems (IROS)*, 2018, pp. 4107–4114.
 - [36] M. Watter, J. Springenberg, J. Boedecker, and M. Riedmiller, “Embed to control: A locally linear latent dynamics model for control from raw images,” in *Advances in Neural Information Processing Systems*, C. Cortes, N. D. Lawrence, D. D. Lee, M. Sugiyama, and R. Garnett, Eds., 2015, pp. 2746–2754.
 - [37] A. M. Wells, N. T. Dantam, A. Shrivastava, and L. E. Kavraki, “Learning feasibility for task and motion planning in tabletop environments,” *IEEE robotics and automation letters*, vol. 4, no. 2, pp. 1255–1262, 2019.
 - [38] D. Xu, R. Martíen-Martíen, D.-A. Huang, Y. Zhu, S. Savarese, and F.-F. Li, “Regression planning networks,” in *Conference on Neural Information Processing Systems*, 2019, pp. 1317–1327.
 - [39] D. Xu, Y. Zhu, C. B. Choy, and L. Fei-Fei, “Scene graph generation by iterative message passing,” in *Proceedings of the IEEE conference on computer vision and pattern recognition*, 2017, pp. 5410–5419.
 - [40] Y. Ye, D. Gandhi, A. Gupta, and S. Tulsiani, “Object-centric forward modeling for model predictive control,” 2019.